Geotechnical Engineering for the Preservation of Monuments and Historic Sites III – Lancellotta, Viggiani, Flora, de Silva & Mele (Eds)

Dynamic centrifuge model tests on Tumulus Mounds on cut slopes

M. Sawada & M. Mimura
Kyoto University, Kyoto, Japan

Tatsuya Udo
Former Student of Kyoto University, Kyoto, Japan

ABSTRACT: Japan's tumulus mounds comprising compacted earth mounds and masonry burial chambers are vulnerable to earthquakes. This study focuses on the seismic behavior of tumulus mounds with sloped foundations. Dynamic centrifuge model tests were conducted using 1/50 scale cross-sectional models of tumulus mounds. The results show that large cracks occurred in the earth mound on the slope side when the shear resistance of the stone joints of the burial chamber was small. The stress distributions in the earth mound during the shaking tests were numerically estimated to identify the stress that caused cracks in the earth mound. The results show that tensile cracks dominantly occur near the surface under low confining pressure. The shear resistance of the stone joints of the burial chamber significantly restrains the opening of the tensile cracks; thus, it is an important factor to be considered when evaluating the seismic resistance of tumulus mounds and developing countermeasures.

1 INTRODUCTION

Historic monuments composed of soil are vulnerable to natural disasters, and their maintenance and restoration require advanced knowledge of geotechnical engineering. Japan has various geo-relics, such as tumulus mounds, kilns, and dwelling sites. Japan's geo-relics have begun to be internationally recognized for their values. The Mozu-Furuichi Kofun Group, consisting of 49 tumulus mounds in Osaka, was included in the UNESCO World Heritage List in 2019, followed by the registration of the Jomon Prehistoric Sites in Northern Japan, which consists of 17 archeological sites including dwelling sites, in 2021. Owing to increased attention to Japan's geo-relics, protecting them from natural disasters is becoming increasingly important.

This study focuses on the damage to tumulus mounds caused by earthquakes. Tumulus mounds were constructed all over Japan from the middle of the 3rd century to the end of the 7th century, and more than 100,000 tumulus mounds have been discovered. Masonry burial chambers are stored in compacted earth mounds of various shapes (e.g. round, rectangular, and keyhole). The length of the earth mounds varies from several meters to approximately 500 m. In the burial chambers, coffins, funerary goods, and mural paintings were preserved in good conditions under a stable hydrothermal environment. Damage to the earth mounds causes the promotion of water and heat transfers, which affects the environment in the burial chambers, thus leading to the deterioration of the burial items owing to dew condensation, salt crystallization, and fungi. This indicates that the role of the earth mounds is to control water and heat transfers into the burial chambers, therefore conserving the burial mounds in good condition. Thus, the mechanical properties and stability of the earth mounds are essential factors to be considered in the conservation of tumulus mounds.

DOI 10.1201/9781003308867-50

In Japan, the tumulus mounds have been repeatedly damaged by earthquakes. During archaeological investigations of tumulus mounds, cracks probably caused by earthquakes have been often discovered. Figure 1 shows the cracks found in the mound of the Takamatsuzuka Tumulus in Nara. Seismological investigations identified the historic earthquakes that caused the cracks as the Nankai Trough Earthquakes, which have periodically occurred in the Pacific Ocean (Agency of Cultural Affairs et al. 2017). However, the details of the damage caused by the earthquakes were unclear because records of historic earthquakes were limited until the occurrence of the Kumamoto Earthquake in 2016 (M = 7.3), which destroyed many tumulus mounds (Agency of Cultural Affairs 2017). Figure 2 shows the Kamao Tumulus in Kumamoto that was damaged by the earthquake. Cracks similar to those shown in Figure 1 were found at the top of the earth mound. Investigations of such seriously damaged tumulus mounds involve risks, and their restoration takes several years. To protect tumulus mounds from future earthquakes, it is necessary to understand the mechanism of seismic damage and develop effective reinforcement measures.

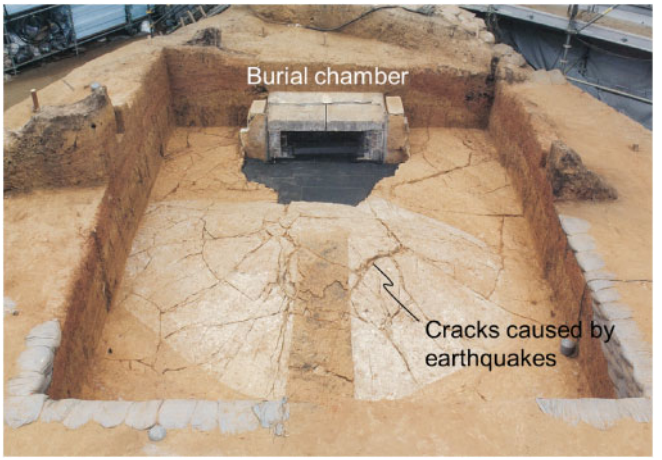

Figure 1. Excavated top of the Takamatsuzuka Tumulus (Agency of Cultural Affairs et al., 2017).

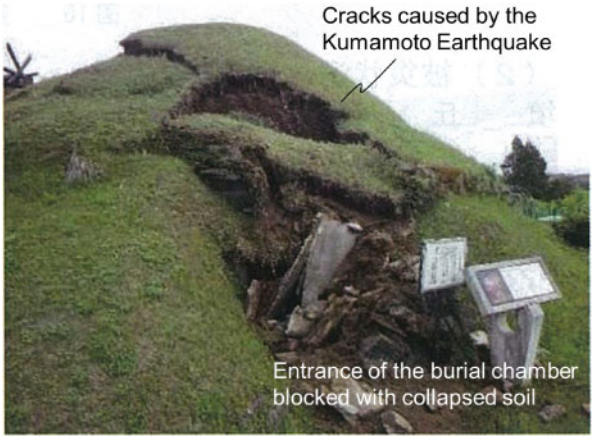

Figure 2. The Kamao Tumulus damaged by the Kumamoto Earthquake (Agency of Cultural Affairs, 2017).

The mechanism of seismic damage to tumulus mounds has been studied using both numerical and experimental approaches. Mimura et al. (2011) conducted three-dimensional FE analyses on the

Takamatsuzuka Tumulus to ensure that the cracks shown in Figure 1 can be caused by earthquakes. Sawada et al. (2018) and Sawada et al. (2019) conducted dynamic centrifuge model tests to observe the damage processes in more detail. The test results were numerically analyzed to identify the stress that caused the damage. These previous studies concluded that cracks are likely to occur near the surface of the earth mounds and corners of the burial chambers, and they are mainly caused by tensile stress.

In the present study, the mechanism of seismic damage to tumulus mounds with sloped foundations is analyzed because significant damage seems to occur, particularly when the foundations are sloped (e.g. Asuka Village Board of Education 2007). Dynamic centrifuge model tests were conducted using 1/50 scale cross-sectional models of tumulus mounds with sloped foundations. In addition, FE analyses were performed to estimate stress distributions in the models during shaking tests. The mechanism of damage and the interactions between the burial chamber and the surrounding earth mound were analyzed based on these results.

2 EXPERIMENT

2.1 *Centrifuge system*

A centrifuge model test is an approach that is widely used to observe the complicated behavior of earth structures caused by earthquakes, seepage, and interactions between soil and structures. The greatest advantage of the centrifuge experiments comes from the equivalence between the physical model and the prototype in terms of stress and strain.

In the present study, the centrifuge system of the Disaster Prevention Research Institute, Kyoto University, was used. The specifications of the system are summarized on the DPRI Geotechnical Centrifuge Center website. The capacity of the centrifuge acceleration was limited to 50 G (1G = 9.81 m/s^2) when a shaking table was used. Thus, in this study, shaking tests were conducted under 50 G using 1/50 models based on the scaling law shown in Table 1. A model created in a rigid aluminum soil box (630 mm × 700 mm × 150 mm) was mounted on the shaking table. The soil box had an acrylic transparent front panel. A high-speed camera was set in front of this outer panel to observe the model during the shaking tests. Centrifuge acceleration was gradually increased until it reached 50 G, and then the shaking table was moved to simulate the preliminary time series data of the input waves.

Table 1. Scaling law of the centrifuge model tests.

Properties	Dimensions	Scale factors (Prototype/Model)
Length	L	N
Mass	M	N^3
Time	T	N
Acceleration	LT^{-2}	N^{-1}
Stress	$ML^{-1}T^{-2}$	1
Strain	–	1

2.2 *Modeling*

Figure 3 shows the 1/50 scale cross-sectional model of the tumulus mound used in this study. The dimensions of the model were determined based on those of the Takamatsuzuka Tumulus (Agency of Cultural Affairs et al., 2017). The tumulus mound was thought to have been created on cut slopes for religious and political reasons. The burial chamber was placed on the flat zone of the foundation, and the earth mound covered the bottom half of the sloped zone. The burial chamber was modeled using four resin plates with a density equal to that of the stones used for the actual

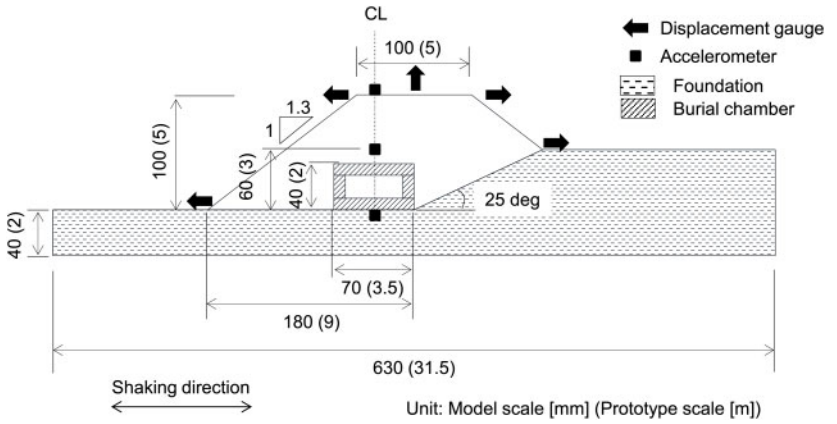

Figure 3. Cross-sectional model of a tumulus mound used for centrifuge model tests.

burial chamber (i.e. 1.91 g/cm^3). The resin plates were rigid and were not bonded each other. The shear resistance between the smooth resin plates was measured using a shear box test (JGS 0561). The results are presented in Table 2. Here, the model composed of smooth resin plates is called Model A.

Table 2. Shear resistance obtained using shear box tests.

Materials	Cohesion [kN/m^2]	Angle of shear resistance [°]
Resin plate – Resin plate (natural)	10.2	17.9
Resin plate – Resin plate (increased roughness)	11.6	32.6
Resin plates – Mound soil	19.0	23.3
Mound soil	21.0	35.0

In addition to Model A, the following two models were used for the experiments: a model without a burial chamber (Model B) and a model with a burial chamber composed of resin plates having interface with increased roughness (Model C). Soil particles were attached to the resin plates used for Model C to increase the shear resistance between the interface between the plates. This surface treatment was not applied to the plate – soil interface. Table 2 compares the shear resistances between the plate interface of Model A and Model C, which indicates that the angle of shear resistance of Model C is 1.8 times as large as that of Model A, while the cohesion of these models is equivalent. The dimensions of these additional models are equivalent to those of Model A, as shown in Figure 3. The influence of the burial chamber on the seismic behavior of the tumulus mound was analyzed by comparing with it these additional cases.

2.3 *Materials and methods*

The models were created using decomposed granite soil (clay: 24.79%, silt: 17.26%, sand: 57.95%) obtained in a tumulus near the Takamatsuzuka Tumulus, where archaeological investigations were conducted. The soil was used after it had passed through a 2-mm sieve. The soil water content was 15%. The densities of the earth mound and foundation soil were determined to have S-wave velocities equal to those measured in the Takamatsuzuka Tumulus, that is, 110–160 and 260–340 m/s, respectively (Mimura & Ishizaki 2006). However, the S-wave velocity of the foundation was far below 260 m/s, despite compacting the soil as densely as possible. Thus, the soil was mixed

with a 10% weight ratio of hydrated lime to achieve the measured S-wave velocity. The properties of the earth mound and foundation are listed in Table 3.

Table 3. Properties of the models used for centrifuge model tests.

Properties	Earth mound	Foundation
Particle density [g/cm^3]	2.64	–
Wet density [g/cm^3]	1.58	1.91
Water content [%]	15	–
Poisson's ratio	0.35	0.35
Shear modulus [MN/m^2]	27	119
S-velocity [m/s]	130	250

The foundation was compacted layer by layer in the soil box. The thickness of each layer was 2 cm. In the sloped zone, a step-like slope was first created using wooden boards as spacers, and then the steps were cut off to smooth the slope. The burial chamber was placed on the flat zone of the foundation, and the earth mound was compacted layer by layer using spacers in the same manner as the foundation. The burial chamber was filled with a block to prevent the resin plates from moving during the compaction of the earth mound. The block was removed after the earth mound was completed.

The displacement and acceleration were measured at the points shown in Figure 3. Laser displacement gauges were attached to the bars fixed at the top of the soil box. L-shaped targets were installed at the top and bottom of the slopes to measure the horizontal displacement of the earth mound. The acceleration in the shaking direction was measured using cubic accelerometers with a side length of 16 mm.

Sinusoidal waves with a frequency of 2 Hz and a duration of 15 s (main part: 20 cycles, tapered part at each end: 5 cycles) in the prototype scale were used as input waves. The amplification was increased step by step from 0.1 to 1.0 mm with an increment of 0.1 mm. Thus, 10 waves with different amplitudes were used for each model.

3 RESULTS

3.1 *Displacement*

Figure 4 shows the models after a series of shaking tests. The earth mound of Model A was significantly damaged with large cracks on the slope side, whereas the other two models were visually the same as those in the initial conditions.

Figure 5 shows the residual displacement accumulated in the 10 shaking tests. Hereinafter, the measurements are described in the prototype scale following the scaling law shown in Table 1. The displacement along the direction of the arrows shown in Figure 3 is positive. The amplitude of the acceleration measured at the shaking table was placed on the horizontal axis. This indicates that the development of displacement in Model A was significant in the 7th shaking test. The earth mound subsided and moved away from the slope of the foundation, as shown in Figure 4. This agrees with the observation made using the high-speed camera. Residual displacement was also observed in the other two models, but its magnitude was small compared to that of Model A, as shown in Figure 5. The right side of the slope of the earth mound in Model B gradually moved to the left in each shaking test. Slight displacement was observed at the crown of the earth mound in Model C, although the large displacement at the left toe of the earth mound in Model C could have been caused by the inclination of the L-shaped target.

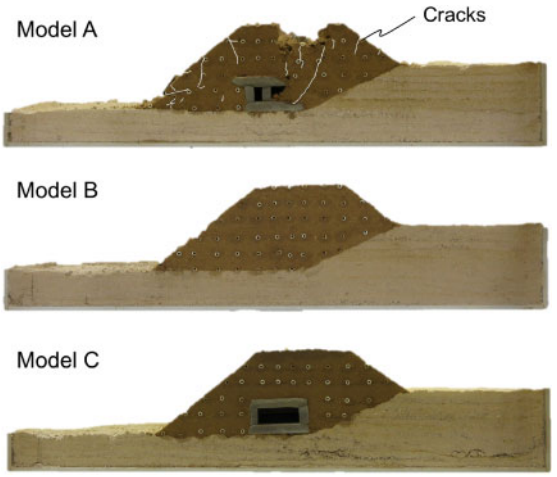

Figure 4. Models after the shaking tests.

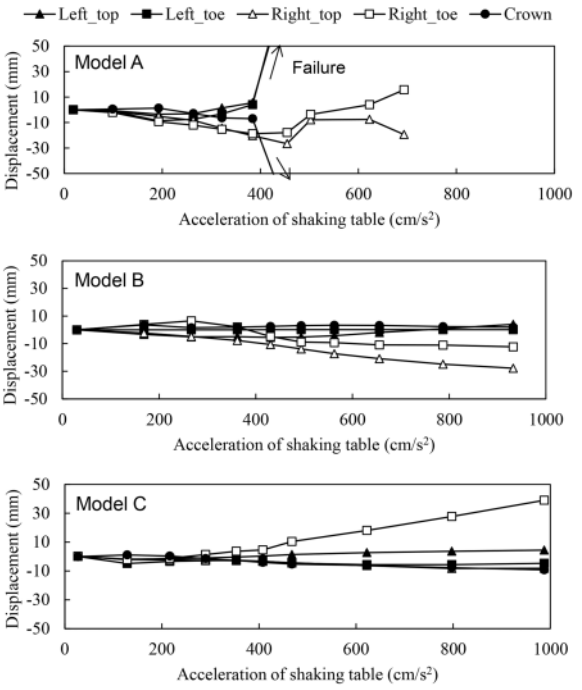

Figure 5. Accumulated residual displacement.

3.2 *Acceleration*

The amplification ratio of each model was obtained from the measured acceleration in the shaking tests using sinusoidal waves. The amplitude ratio $A_{r/s}$ is defined as follows:

$$A_{r/s} = Z_r / Z_s \tag{1}$$

where Z_s is the Fourier amplitude of the acceleration measured on the foundation surface, and Z_r is the acceleration measured at the three points shown in Figure 3. Herein, the Fourier amplitude at 2 Hz was used to calculate $A_{r/s}$, although the measured acceleration contained waves with higher frequency coming from the actuator system of the shaking table.

Table 4 shows the average amplitude ratio at the three points of each model using the results of the 1st to the 5th shaking tests. The amplitude ratio increases with an increase in elevation between the bottom (i.e. foundation surface) and middle points, but it slightly decreases between the middle and top (i.e. crown) points. Comparisons of the amplitude ratio between the three models indicate that the burial chamber increases the amplification in the earth mound, particularly when the shear resistance of the plate joints of the burial chamber is small.

Table 4. Amplitude ratio.

	Middle	Top
Model A	1.31	1.19
Model B	1.20	1.15
Model C	1.24	1.20

4 DISCUSSION

4.1 *Numerical analyses*

FE analyses were conducted to understand the damage mechanism observed in Model A. A two-dimensional FE code LIQCA 2018 (Liquefaction Geo-Research Institute, 2018), which implements a modified Ramberg-Osgood model (e.g. Ishihara, 1996), was used. The model is a total stress model that considers nonlinear stress-strain relationships in cyclic loading. The model parameters α and r were determined to be 7.84 and 2.29 by fitting to the results of cyclic triaxial tests (JGS 0542), that is, shear strain versus shear modulus and shear strain versus damping constant. The determination of the model parameters was detailed by Sawada et al. (2018). The FE model shown in Figure 6 was created in the prototype scale, which corresponds to the model shown in Figure 3 above foundation surface level. The acceleration measured at the foundation surface was provided at the bottom of the FE model. The lower part of the foundation was not included in the numerical model because trial calculations using a numerical model with a full foundation showed that it causes the discrepancy between measured and simulated acceleration in the earth mound. The discrepancy can come from uncertainties of the physical models such as the boundary conditions between the shaking table and soil box, or the soil box and foundation. The resin plates of the burial chamber were assumed to be rigid. The slip and gap between the plates or between the plates and soil were considered using joint elements (Goodman et al. 1968). A joint element consists of horizontal and vertical springs that express slip and gap, respectively. These springs have bilinear stress-strain curves. The parameters of the horizontal springs were determined by fitting to the

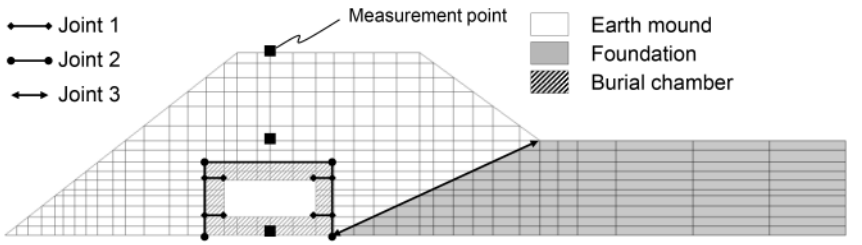

Figure 6. Numerical model (Model A).

stress-strain curves obtained by shear box tests. The vertical spring constant was determined to be as large as possible, and the tensile strength was assumed to be zero. Joint elements were also applied to the boundary between the slope of the foundation and the earth mound, assuming that they had shear strength of the earth mound. The model parameters of the joint elements are listed in Table 5.

Table 5. Model parameters of joint elements.

Parameters		Model A	Model B	Model C
Joint 1				
Horizontal	Spring constant [kN/m^2]	6.0×10^5	–	6.0×10^5
	Cohesion [kN/m^2]	10.2	–	11.6
	Angle of shear resistance [°]	17.9	–	32.6
Vertical	Spring constant [kN/m^2]	1.0×10^7	–	1.0×10^7
	Tensile strength [kN/m^2]	0.0	0.0	0.0
Joint 2				
Horizontal	Spring constant [kN/m^2]	4.5×10^4	–	4.5×10^4
	Cohesion [kN/m^2]	19.0	–	19.0
	Angle of shear resistance [°]	23.3	–	23.3
Vertical	Spring constant [kN/m^2]	1.0×10^6	–	1.0×10^6
	Tensile strength [kN/m^2]	0.0	0.0	0.0
Joint 3				
Horizontal	Spring constant [kN/m^2]	6.0×10^4	6.0×10^4	6.0×10^4
	Cohesion [kN/m^2]	21.0	21.0	21.0
	Angle of shear resistance [°]	35.0	35.0	35.0
Vertical	Spring constant [kN/m^2]	1.0×10^6	1.0×10^6	1.0×10^6
	Tensile strength [kN/m^2]	0.0	0.0	0.0

Figure 7 shows the comparison between the measured and calculated accelerations in the 2nd, 4th and 7th shaking tests. The calculated acceleration agrees well with the measured acceleration in the 2nd and 4th tests. In the second half of the 7th shaking test, the measured acceleration had a phase lag and noise because the crack opening in the earth mound became significant. Numerical analyses were also conducted for Model B and Model C in the same manner as for Model A. The measured accelerations of these two models were also numerically simulated using common model parameters.

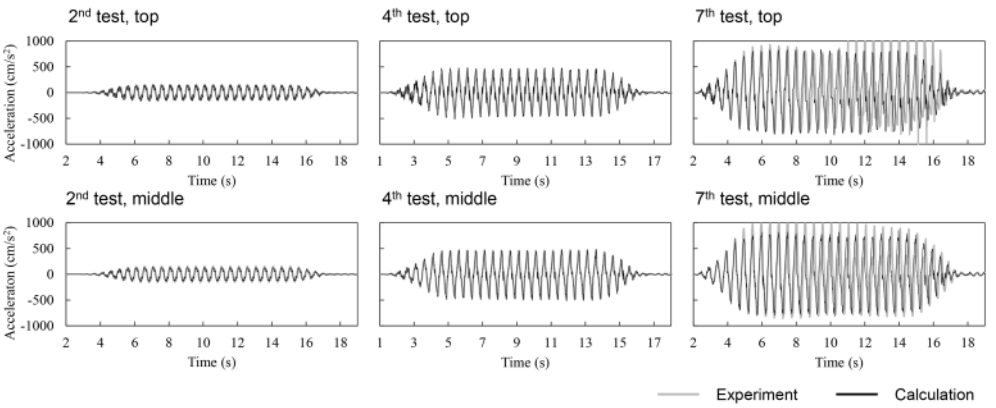

Figure 7. Comparison between measured and calculated acceleration (Model A).

4.2 *Mechanism of damage*

Figures 8 and 9 show the distributions of the calculated maximum shear stress and maximum tensile stress (i.e. negative minimum principal stress) in the earth mound when they peak in most parts during the 11th cycle during the 7th shaking test. This indicates that shear stress develops in the deep zone, particularly around the burial chamber, whereas tensile stress develops near the surface. The tensile stress distribution of Model A was characterized by a band of large tensile stress on the slope side. The band appeared throughout the shaking tests, and its position corresponded to the portion where a significant crack occurred in the experiment (Figure 4). This suggests that the cracks were caused by tensile stress. The tensile band is moderate in Model C, with a large shear resistance of plate joints.

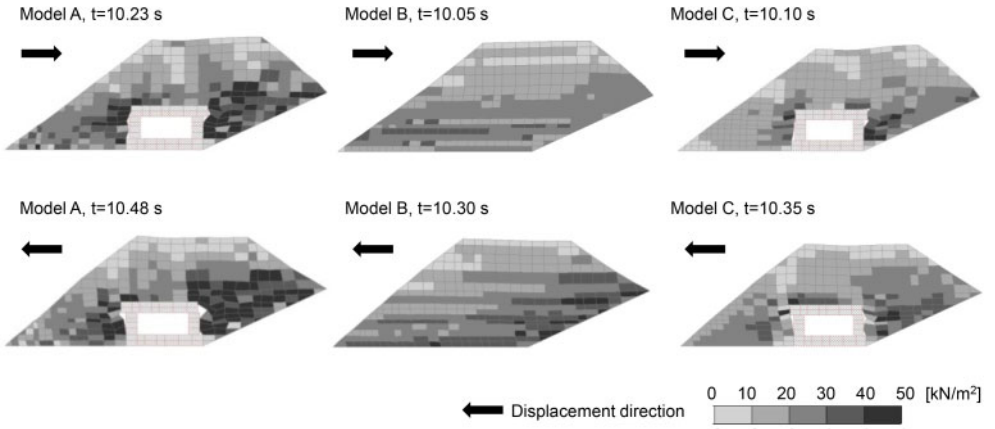

Figure 8. Distribution of maximum shear stress.

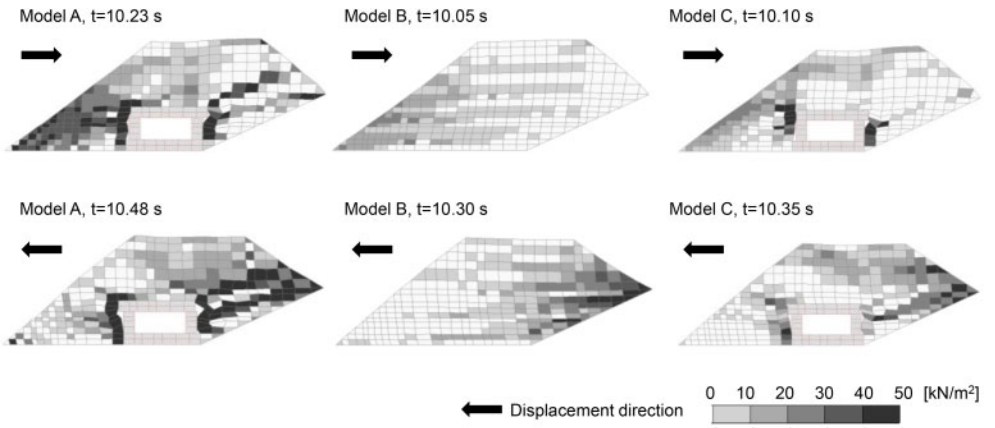

Figure 9. Distribution of maximum tensile stress.

The stress planes of the maximum shear stress and tensile stress were identified for the elements, in which these stresses reached thegir strengths until the 11th cycle in the shaking tests. The shear strengths of the earth mound are listed in Table 2. The tensile strength was estimated to be less than 20 kPa based on the modified Mohr-Coulomb failure criterion (e.g. Sawada et al. 2021). However, such a small tensile strength cannot be exactly measured with conventional tension tests, and thus, it was assumed to be zero. Figure 10 shows the distributions of the directions of these

stress planes. This is useful for identifying the stress that caused cracks in Model A. The directions of the experimentally observed cracks seem to be consistent with the estimated directions of the stress plane of the maximum tensile stress and not those of the maximum shear stress. In addition, shear failure was estimated not to occur at the top of the earth mound, although many cracks were found, as shown in Figure 4. These results show that the cracks were mainly caused by tensile stress. Tensile cracks are unique to unsaturated soils under low confining pressures with apparent cohesion and tensile strength induced by matric suction.

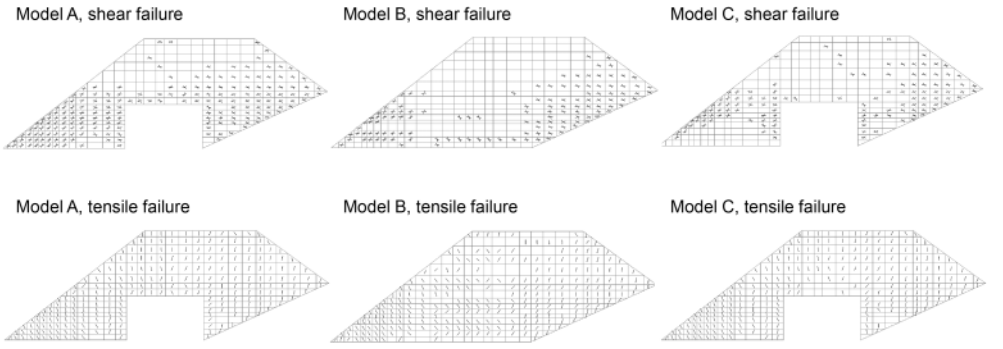

Figure 10. Directions of the planes where shear failure and tensile failure occur.

Tensile cracks were also estimated to occur in Model B and Model C, as shown in Figure 10 where the tensile stress was assumed to be zero. This indicates that tensile failure occurred in these models; however, cracks were invisible because the crack opening was moderate, which was consistent with the fact that a small but detectable residual displacement was measured, as shown in Figure 5. Figure 11 shows the numerically estimated horizontal relative displacement between the ceiling plate and right-side wall plate of the burial chamber of Model A and Model C in the 2nd, 4th, and 7th shaking tests. This indicates that the slip between these plates was restrained in Model C, which prevented crack opening and serious damage to the earth mound. Thus, the shear

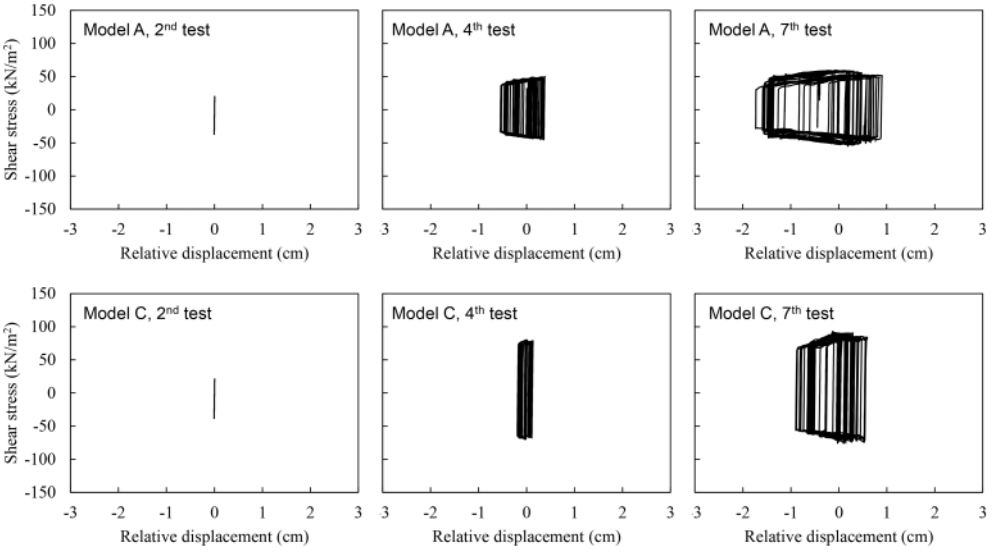

Figure 11. Relative displacement of the joint element between the ceiling and right-side wall.

resistance of the stone joints of burial chambers is an important factor in evaluating the seismic resistance of tumulus mounds. In addition, an increase in the shear resistance can be an effective measure for protecting tumulus mounds from earthquakes.

5 CONCLUSION

This study focuses on the seismic behavior of tumulus mounds with sloped foundations, which are particularly vulnerable to earthquakes. Dynamic centrifuge model tests were conducted using a 1/50 scale cross-sectional model of a tumulus mound. The results show that the damage to the earth mound is characterized by large cracks on the slope side when the stone joints of the burial chamber have a small shear resistance. The measured acceleration shows that the amplification ratio of the earth mound is influenced by whether the earth mound has a burial chamber and the magnitude of the shear resistance of the stone joints of the burial chamber.

The shaking tests were numerically analyzed to understand the mechanism of the experimentally observed damage in the earth mound. The distributions of the maximum shear stress and tensile stress were numerically estimated to identify the stress that caused the large cracks. The results show that the distribution and direction of the maximum tensile stress correspond closely to those of the large cracks. This indicates that the earth mound has apparent cohesion and tensile strength induced by matric suction, and tensile failure dominantly occurs near the surface under low confining pressure. The numerical results also show that the shear resistance of the stone joints of the burial chambers is an important factor in evaluating the seismic resistance of tumulus mounds and developing protection measures.

REFERENCES

Agency for Cultural Affairs, Nara National Research Institute for Cultural Properties, Archeological Institute of Kashihara Nara prefecture & Asuka Village Board of Education. 2017. Excavations report in the Takamatsuzuka Tumulus: 155–160 (in Japanese).

Agency for Cultural Affairs. 2017. Report on tumuli damaged by the 2016 Kumamoto Earthquake (in Japanese).

Asuka Village Board of Education. 2007. Excavations report in Kazumayama Tumulus (in Japanese).

DPRI Geotechnical Centrifuge Center. https://sites.google.com/dpri.kyoto-u.ac.jp/centrifuge/home/souchishiyou?authuser=0 (accessed 2021-10-11)

Goodman, R. E., Taylor, R. L., & Brekke, T. L. 1968. A model for the mechanics of jointed rock. *Journal of the soil mechanics and foundations division*, 94(3): 637–659.

Ishihara, K. 1996. Soil behaviour in earthquake geotechnics, *Oxford engineering science series 46*: 33–39.

Japanese Geotechnical Society Standards, 2015. Laboratory testing standards of geomaterials-Part 1, Method for consolidated constant-pressure direct box shear test on soils (JGS 0561).

Japanese Geotechnical Society Standards, 2017. Laboratory testing standards of geomaterials-Part 2, Method for cyclic triaxial test to determine deformation properties of geomaterials (JGS 0542).

Liquefaction Geo-Research Institute. 2018. Theories and manuals for LIQCA2D18 and LIQCA3D18 (in Japanese).

Mimura, M. & Ishizaki, T. 2006. Current status of Takamatsuzuka Tumulus and its geotechnical properties, *Japanese Geotechnical Journal*, 1 (4): 157–168 (in Japanese).

Mimura, M., Nagaya, J. & Ishizaki, T. 2011. Evaluation of seismic damage to the mound of Takamatsuzuka Tumulus based on dynamic finite element analysis, *Conservation Science* 50: 13–22 (in Japanese).

Sawada, M., Enkhtuvshin, T. Mimura, M. 2018. Study on the seismic behavior and damage mechanism of tumulus mounds, *Journal of Japan Society of Civil Engineers, Ser. C (Geosphere Engineering)*, 74 (3): 374–387 (in Japanese).

Sawada, M., Enkhtuvshin, T. Mimura, M. 2019. Study on the mechanism of seismic damage of historical burial mounds, *Proc. 16th Asian Regional Conference*, ATC19-3.

Sawada, M., Sumi, Y. & Mimura, M. 2021. Measuring desiccation-induced tensile stress during cracking process, *Soils and Foundations*, 61 (4): 915–928.